Weak magnetic flux leakage: a possible method for studying pipeline defects located either inside or outside the structures

B. Liu [1], Y. Chao [1], H. Zhang [2], Y.R. Lin [1], W.R. Sun[1], B. Xu [3]

1(School of Information Science and Engineering，Shenyang University of Technology，Shenyang，110870，China)

2(Computer Vision and Systems Laboratory, Department of Electrical and Computer Engineering, Université Laval, 1065, av. de la Médecine, Québec, QC G1V 0A6, Canada)

3(Information Technology Department, Shenyang Polytechnic College, Shenyang 110045, China)

Abstract： Magnetic leakage distribution results from linear defects of oil-gas pipelines in a weak magnetic field, which is modeled by the magnetic dipole theory. The analysis is useful for the identification of defects located either inside or outside the pipelines. The results indicate that the radial signals of inside-outside defects can be clearly distinguished, and the axial signals are basically the same in a weak magnetic field. The theoretical and the experimental results are very consistent.

Key Words: magnetic leakage; magnetic dipole; weak magnetic field; inside-outside defects

Corresponding author. Tel. 0086-024-77818528，13998284051

E-mail address: syuotwenwu@sina.com (Bin Liu)

Oil and gas pipeline transportation plays a very important role in our national economy, and is referred to as "the main artery of energy circulation". With the increase in service time, there exists a great potential risk for pipelines which may suffer from corrosion and damage caused by external forces and other problems. Among the traditional non-destructive testing methods, magnetic flux leakage (MFL) is the most popular method for in-line inspection of pipelines [1-3]. The MFL method can successfully overcome physical and practical inspection challenges presented by transmission pipelines, and MFL inner detector has been used to detect and measure corrosion defects, mechanical damages and cracks [4-6]. However, some questions are not solved completely, such as estimating flaw size, defect shape, the difference of

inner-outer defects and so on [7, 8]. Therefore, to improve the estimation precision of defects, many approaches have been studied. In this paper, we will provide a brief background on the weak magnetic field model to discuss the inspection and identification of inner-outer defects on oil-gas pipelines. The experiments carried out herein indicate that it is feasible to distinguish inner and outer defects. These results can provide a scientific basis for the improvement and practical application of the traditional pipeline MFL testing method.

1 Principle and Basic structure

The MFL testing system is widely used to detect metal losses of the oil-gas pipelines [10-12]. In the system, the detecting module consists of a permanent magnet, magnetic yoke and Hall sensors. As shown in Fig.1, the pipeline of interest is magnetized by a magnetic system with a permanent magnet and yoke to reach magnetic saturation, and then Hall sensors detect the leakage fields in the metal loss area.

All detected signals are sent to the computer by a USB interface. Fig. 2 shows the variation of the magnetic field, which can be achieved through the movement of the inner detector at a measured point. As the detector passes, the magnitude and direction of the magnetic field at the measured area is set out.

2 Mathematical model of leakage field distribution

The magnetic dipole is a basic magnetic unit. With characteristics of a different physical meaning and a clear geometric image, the magnetic dipole theory can be used to solve some theoretical problems in the traditional magnetic NDT area.

According to Coulomb’s law, the model is established at a place which is deduced by the infinity analyzed object and the far magnetic field formula of the dipole. However, MFL testing is carried out in the near surface of the magnetic charges, only involving the field characteristics. Therefore, the approximate solution of the far field has to be a small reference value, and the exact solution is suitable for

investigating the near field characteristics of the magnetic dipole.

Under a strong magnetic field, the MFL signal depends mainly on the external magnetic field. It can be simulated by simplified two-dimensional models based on axisymmetric structures of pipelines. In a cylindrical coordinate system $(r\ \theta\ z)$, Maxwell differential equations for the analysis of a static magnetic field are as follows:

$$\frac{\partial}{\partial r}\left[\frac{1}{r}\frac{\partial}{\partial r}(r\cdot A)\right]+\frac{\partial^2 A}{\partial Z^2}=-\mu J \qquad (1)$$

Magnetic scalar and exciting current density only have circumferential components and can be regarded as scalars, and then the energy function equation can be created by a finite element model to solve the minimum of space energy, namely,

$$F(A)=2\pi\iint_s\frac{1}{2\mu}B^2\cdot rd_rd_z-2\pi\iint_s JArd_rd_z+2\pi\int_{L_2}\frac{1}{\mu}\left[\frac{1}{2}fA_1^2-fA_2\right]rd_l \qquad (2)$$

Where, f expresses the exciting source of the magnetic field, s represents the magnetic field required, L_2 shows the boundary of the magnetic field space, $F(A)$ denotes the function equation, r refers to the radius and A_1、A_2 represents the boundary values of the magnetic field space. The models can be subdivided by a two-dimensional region Delaunay program. In any small unit e, vector magnetic potential can be shown as:

$$A=a_1+a_2r+a_3z \qquad (3)$$

The magnetic potential values $A_i(r_i,z_i)$, $A_j(r_j,z_j)$ and $A_m(r_m,z_m)$ on three nodes can be substituted into Eq.（3）:

$$\begin{vmatrix}\alpha_1\\ \alpha_2\\ \alpha_3\end{vmatrix}=\frac{1}{2\Delta}\begin{vmatrix}\alpha_i & \alpha_j & \alpha_m\\ \alpha_i & \alpha_j & \alpha_m\\ \alpha_i & \alpha_j & \alpha_m\end{vmatrix}=\frac{1}{2\Delta}\begin{vmatrix}r_jz_m-r_mz_j & z_j-z_m & r_m-r_j\\ r_mz_i-r_iz_m & z_m-z_i & z_i-z_m\\ r_iz_j-r_jz_i & z_i-z_j & z_j-z_i\end{vmatrix} \qquad (4)$$

Where, $\Delta=\frac{1}{2}(b_ic_j-b_jc_i)$, α_1,α_2 and α_3 in Eq. (4) can be substituted into Eq. (3), and then Eq. (5) can be obtained as follows:

$$A^e = A_i N_i^e + A_j N_j^e + A_m N_m^e \tag{5}$$

Where, A^e refers to the magnetic potential, $A_l (l = i, j, m)$ represents the coefficient of the basis function $N_l (l = i, j, m)$. In the unit e, B_r^e and B_z^e can be obtained for an axisymmetric pipeline system as follows:

$$B_r^e = -\alpha_3 \tag{6}$$

$$B_z^e = \frac{A}{r} + \alpha_2 \approx \frac{A^e}{r^e} + \alpha_2 \tag{7}$$

Where, $r^e = \frac{1}{3}(r_i + r_j + r_m)$ and $A^e = \frac{1}{3}(A_i + A_j + A_m)$ are values in the center of e, so $[B^2]^e$ can be expressed as:

$$[B^2]^e = \alpha_2^2 + \alpha_3^2 + 2\alpha_2 \frac{A^e}{r^e} + \left|\frac{A^e}{r^e}\right|^2 \tag{8}$$

So $F(A)$ can be written as follows:

$$F(A) \approx \sum_{e=1}^{h} F^e(A) = \sum_{e=1}^{h} \left| 2\pi \iint_s \frac{1}{2\mu} [B^2]^e r d_r d_z - 2\pi \iint_s JA r d_r d_z \right| + 2\pi \int_{L_2} \frac{1}{\mu} \left[\frac{1}{2} f A_1^2 - f A_2 \right] r d_l$$
$$= \sum_{e=1}^{h} (F_1^e + F_2^e) + F_3^e \tag{9}$$

F_1^e and F_2^e can be obtained by the following:

$$F_1^e(A) = \frac{1}{2}[A_i \quad A_j \quad A_m] \begin{vmatrix} k_{ii} & k_{ij} & k_{im} \\ k_{ji} & k_{jj} & k_{jm} \\ k_{mi} & k_{mj} & k_{mm} \end{vmatrix} \begin{vmatrix} A_i \\ A_j \\ A_m \end{vmatrix} = \frac{1}{2}[A]^{e^T}[k]^e[A]^e \tag{10}$$

$$F_2^e(A) = [A_i \quad A_j \quad A_m] \begin{vmatrix} \frac{2\pi}{3} J_0 r^e \Delta \\ \frac{2\pi}{3} J_0 r^e \Delta \\ \frac{2\pi}{3} J_0 r^e \Delta \end{vmatrix} = [A]^{e^T}[P]^e \tag{11}$$

Boundary unit coefficient matrixes on the inhomogeneous natural boundary can be shown as:

$$[K]^e+[K']^e=\begin{vmatrix} K_{ii}^e & K_{ij}^e & K_{im}^e \\ K_{ji}^e & K_{jj}^e+\dfrac{\pi\varepsilon l_0 f_1}{2}\left|r_i+\dfrac{r_m}{3}\right| & K_{jm}^e+\dfrac{\pi\varepsilon l_0 f_1}{2}\left|r_i+\dfrac{r_m}{3}\right| \\ K_{mi}^e & K_{mj}^e+\dfrac{\pi\varepsilon l_0 f_1}{2}\left|r_i+\dfrac{r_m}{3}\right| & K_{mm}^e+\dfrac{\pi\varepsilon l_0 f_1}{2}\left|r_i+\dfrac{r_m}{3}\right| \end{vmatrix} \quad (12)$$

So the exciting matrix can be represented as follows:

$$[P]^e+[P']^e=\begin{vmatrix} \dfrac{2\pi}{3}J_0 r^e\Delta \\ \dfrac{2\pi}{3}J_0 r^e\Delta \\ \dfrac{2\pi}{3}J_0 r^e\Delta \end{vmatrix}+\begin{vmatrix} 0 \\ \dfrac{\pi\varepsilon l_0 f_2}{2}\left|r_i+\dfrac{r_m}{2}\right| \\ \dfrac{\pi\varepsilon l_0 f_2}{2}\left|r_i+\dfrac{r_m}{2}\right| \end{vmatrix} \quad (13)$$

Where, l_0 refers to the boundary length of each small unit. The system of linear equations about A_l on n nodes can be obtained by using the extremes of $F(A)$ to provide the following:

$$\frac{\partial F(A)}{\partial A_l}=0 \quad (14)$$

$$\begin{vmatrix} k_{11} & k_{12} & \cdots & k_{1n} \\ k_{11} & k_{11} & \cdots & k_{11} \\ \vdots & \vdots & \ddots & \vdots \\ k_{11} & k_{11} & \cdots & k_{11} \end{vmatrix}\begin{vmatrix} A_1 \\ A_2 \\ \vdots \\ A_n \end{vmatrix}=\begin{vmatrix} P_1 \\ P_2 \\ \vdots \\ P_n \end{vmatrix} \quad (15)$$

$k_{ij}=\sum_{e=1}^{h}\left|k_{ij}^e+k_{ij}^{e'}\right|$, $P_i=\sum_{e=1}^{h}\left|P_i^e+P_i^{e'}\right|$ and A_l can be obtained by solving Esq.(15).

However, under a weak magnetic field, the material's inherent magnetic moment cannot be ignored. The MFL signal depends on both external magnetic field and the atomic magnetic moment. According to the criterion of Stoner [17]:

$$B=\mu_0(H+M)=\mu_0\{H+N\mu_B[\rho(E)_\uparrow-\rho(E)_\downarrow]\} \quad (16)$$

Where, N is the number of electrons, μ_B denotes atomic magnetic moments, H expresses the external magnetic field, $\rho(E)_\uparrow$ is the spin-up density of states, and $\rho(E)_\downarrow$ is the spin-down density of states.

When the external magnetic field is weak, it can be predicted through Eq. (16). Because the atomic magnetic moment is related to crystal institutions, and the influence of inner-outer defects on the internal surface's crystal institutions are different; so under a weak magnetic field, MFL signals of inner-outer flaws can be distinguished.

3 Model validation and result analysis

3.1 Model validation

The weak magnetic field detection environment can be achieved by adjusting the relative position among defects, magnetic poles and sensors. The magnetic field intensity cannot be too weak; otherwise the MFL signal is easily affected by the earth's magnetic field or may even be undetectable due to the strength of the earth's magnetic field. Fig. 3 shows the distributions of radial component B_x and axial component B_y along the defect direction. The width of the defect zone is 2mm, the lift-off measured value（the vertical distance from the surface of the specimen) is 50 mm and the horizontal distance from the defect is 225mm. All results are normalized by the peak value. Some basic phenomena are clearly observed in MFL tests and are thus observed in the present experiments. For example, B_y exhibits a peak and B_x changes its polarity in the middle position. In the same testing environment, signals are measured by sensors, and the maximum error of B_X is 0.066 T and the maximum error of B_Y is 0.022 T. Due to the geomagnetic disturbance and surroundings, the experimental signals and simulation signals basically coincide, thereby suggesting that the finite element simulation model is correct.

3.2 Result analysis

3.2.1 The weak magnetic field signal dependence on defect depth

Under a strong magnetic field, the length of the defect is a constant value. The peak-peak value $B_X(T-T)$ of the radial MFL signal amplifies with the increase of

defect depth, showing a linear relationship, and the peak value $B_Y(Top)$ of the axial MFL signal is the expected value, according to the law (linear relationship) [18-21]. But under a weak magnetic field, $B_X(T-T)$ and $B_Y(Top)$ reflect a nonlinear relationship.

The width of the inner defect is a constant value (10mm). And the depth of the pipe wall thickness changes from 10% to 50%, the interval is 5%. As shown in fig.4（a）and (b), when the defect depth reaches 40% of the pipe wall thickness, $B_Y(Top)$ appears maximum, and when the defect depth is less than 20% of the wall thickness, $B_Y(Top)$ does not significantly change and the detection signal is invalid. Moreover, when the defect depth is 40% of the wall thickness, $B_X(T-T)$ is at a minimum value.

In the same way, the signal characteristics of outer defects are clearly different. As shown in fig.4(c) and (d), as the depth reaches 50% of the pipe wall thickness, $B_Y(Top)$ reaches a maximum, but when the defect depth is less than 25% of the wall thickness, $B_Y(Top)$ does not significantly change and the signal is invalid. Meanwhile, $B_Y(Top)$ amplifies with the increase of defect depth, which reflects a linear relationship. And when the defect depth is 30% of the wall thickness, $B_X(T-T)$ reaches a maximum value.

3.2.2 The weak magnetic field signal dependence on defect width

When the depth of the inner defect is a constant value (10mm), the width changes from 2mm to 10mm, and the interval is 2mm. As shown in fig.5 and fig.6, axial signals of inner-outer defects increase with the linear relation of the defect's width and the curves in the graph basically coincide. When the defect width is less than 8 mm, radial signals of inner and outer defects basically coincide. However, when the defect's width is greater than 8 mm, the radial signal of the inner defect significantly changes and the trend is obviously different in comparison to that of the outer defect's

signal. In the model, when the defect width is greater than 8 mm, the inner and outer defects can be identified.

4 Experimental analysis

In order to confirm the difference between the inner and the outer defect MFL signals in the weak magnetic environment, the weak magnetic detection system is established as shown in fig.7. Online measuring of the inner -outer defects indicated that the defect's length is 30 mm, the width is 10 mm, and the depth of the pipe wall's thickness is 25%.

As shown in Fig.8 and Fig.9, in a weak magnetic condition, the axial MFL signals in the through-hole, and inner-outer defects' signals are basically the same, but radial signals are clearly different. Thus, the weak magnetic detection method provides the advantage of enabling inner -outer defect discernment in pipelines.

5 Conclusions

Under strong magnetic fields, the MFL signals mainly depend on external magnetic field. The resistance effect of the atomic magnetic moment of the ferromagnetic component can be ignored, and internal and external defects cannot be distinguished. However, under weak magnetic fields, the material's inherent magnetic moment cannot be ignored, the MFL signal depends on both external magnetic field and the atomic magnetic moment, and radial components of inner-outer defects have different distribution trends and inner-outer defects can be distinguished. A new method is put forward for inner-outer defects' testing of pipelines, but the weak magnetic signal is related to the material, wall thickness, diameter, and other factors.

References

[1] Z.J. Wan, J.B. Liao, Y.K. Wang, G.F. Yin. Research on metal tubing pit corrosion monitoring based on potential-array method, Chinese Journal of Scientific Instrument, 2011, 32(1): 19-25.

[2] R. Pohl, A. Erhard, H.J. Montag, H.M. Thomas, H. Wüstenberg. NDT techniques

for railroad wheel and gauge corner inspection, NDT&E International, 2004, 37(2): 89-94.

[3] A. Sophian, G.Y. Tian, S. Zairi. Pulsed magnetic flux leakage techniques and applications, Sensors and Actuators A: Physical, 2006, 125(2): 186-191.

[4] J.H. Liu, J. Feng, Research on leak fault intelligent detection method for fluid pipeline based on fuzzy classification, Chinese Journal of Scientific Instrument, 2011, 32(1): 26-32.

[5] G. Sposito, C. Ward, P. Cawley, P.B. Nagy, C. Scruby. A review of non-destructive techniques for the detection of creep damage in power plant steels, NDT&E International, 2010, 43: 555-567.

[6] W.X. Gao, Y.H. Hu, X.Y. Mu, X.M. Wu. Real-time detection and segmentation of submerged-arc welding defects in X-ray radiography images, Chinese Journal of Scientific Instrument, 2011, 32(6): 1215-1224.

[7] V. Sukhorukov. Magnetic Flux Leakage Testing Strong or Weak Magnetization, Material Evaluation, 2013, 5(7): 26-31.

[8] Y.L. Ma, L. Lin. Research on internal and external defect identification of drill pipe based on weak magnetic inspection, Insight, 2014, 56: 31-34.

[9] F.Y. Xu, X.S. Wang, H.T. Wu. Inspection method of cable-stayed bridge using magnetic flux leakage detection: principle, sensor design, and signal processing, Journal of Mechanical Science and Technology. 2012, 26(3): 661-669.

[10] V. Babbar and L. Clapham. Residual magnetic flux leakage: a possible tool for studying pipeline defects, Journal of Nondestructive Evaluation, 2003, 22(4): 23-33.

[11] F. Forster. New findings in the field of non-destructive magnetic leakage field inspection, NDT&E International, 1986, 19: 3–14.

[12] H.R. Weischedel. The inspection of wire ropes in service: A critical review, OIPEEC Bulletin, 1989, 58: 49–57.

[13] R.K. Stanley. Simple explanation of the theory of the total magnetic-flux method for the measurement of ferromagnetic cross-sections. NDT&E International, 1997, 30: 35.

[14] S. Mandayam, L. Udpa, S.S. Udpa, W. Lord. Wavelet-based permeability

compensation technique for characterizing magnetic flux leakage images. 1997, NDT&E International, 30: 297–303.

[15] D.L. Zhang, M. Zhao, Z.H. Zhou, S.M. Pan. Characterization of Wire Rope Defects with Gray Level Co-occurrence Matrix of Magnetic Flux Leakage Images, Journal of Nondestructive Evaluation, 2013, 32(1): 37-43.

[16] S.F. Garanin. Discharge accompanying leakage of magnetic flux from plasma into an insulator, Journal of Applied Mechanics and Technical Physics, 1987, 28(6): 816-819.

[17] Y. Kakehashi, M.A.R. Patoary. First-principles dynamical coherent-potential approximation approachto the ferromagnetism of Fe, Co, and Ni. Journal of the Physical Society of Japan, 2011, 11(3): 1683-1694.

[18] Y. Yamaguchi, Y. Katada, T. Itou, Y. Uesugi, Y. Tanaka, T. Ishijima. Experimental investigation of magnetic arc blow in plasma arc cutting, Welding in the World, 2015, 59(1): 45-51.

[19] C.G. Stefanita. Magnetic nondestructive testing techniques, Magnetism, 2012, 69-106.

[20] V.V. Davydov, E.N. Velichko, V.I. Dudkin, A. Yu. Karseev. A nutation nuclear-magnetic teslameter for measuring weak magnetic fields, Measurement Techniques, 2014, 57(6): 684-689.

[21] X.M. Li, H.S. Ding, S.W. Bai. Research on the stress-magnetism effect of ferromagnetic materials based on three-dimensional magnetic flux leakage testing, NDT&E International, 2014, 62: 50-54.

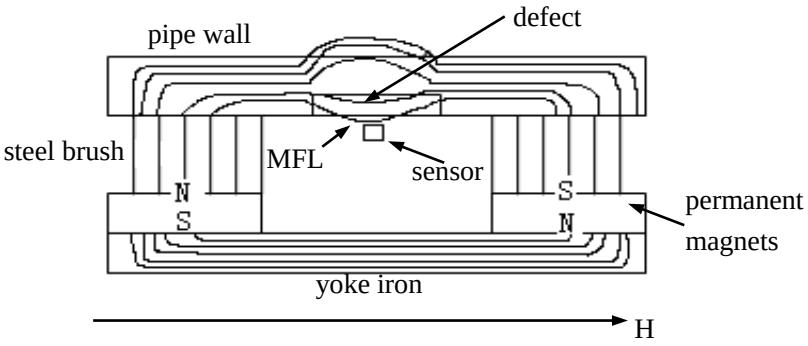

Fig.1 Pipeline MFL detection main magnetic circuit

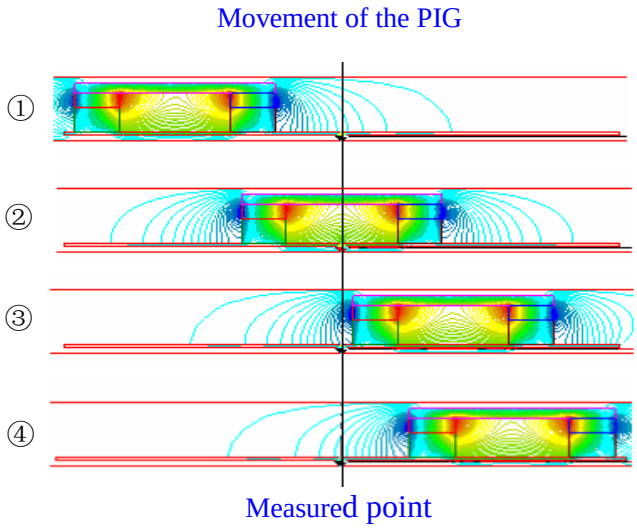

Fig.2 Magnetic fields change according to the movement of the MFL Detector

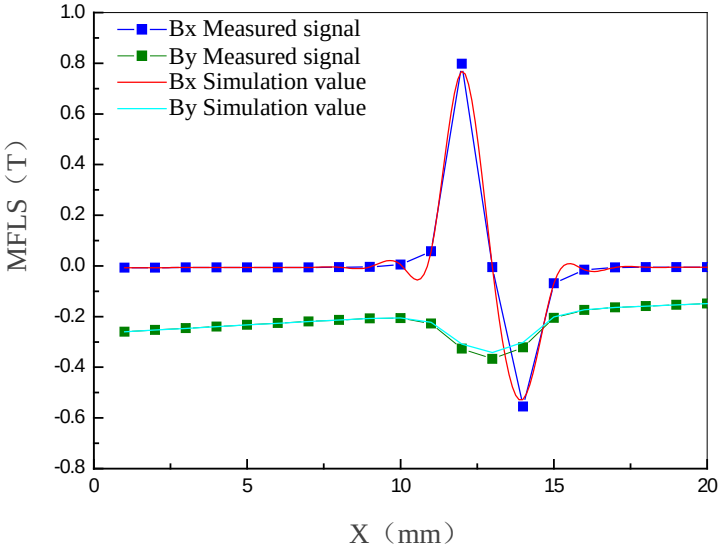

Fig.3 The contrast between measured signal value and simulation value

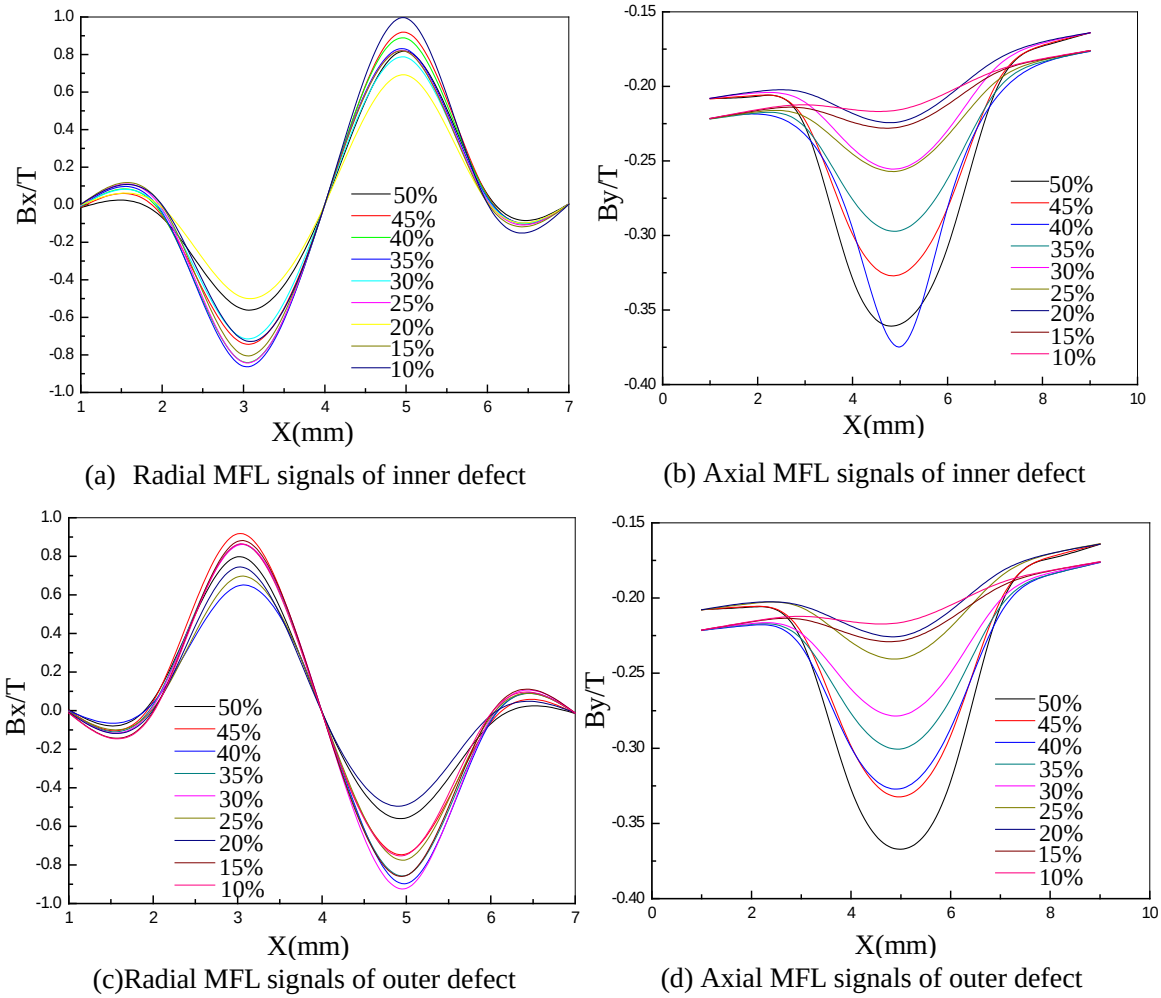

(a) Radial MFL signals of inner defect

(b) Axial MFL signals of inner defect

(c)Radial MFL signals of outer defect

(d) Axial MFL signals of outer defect

Fig.4 Weak magnetic field signals dependence on defect depth

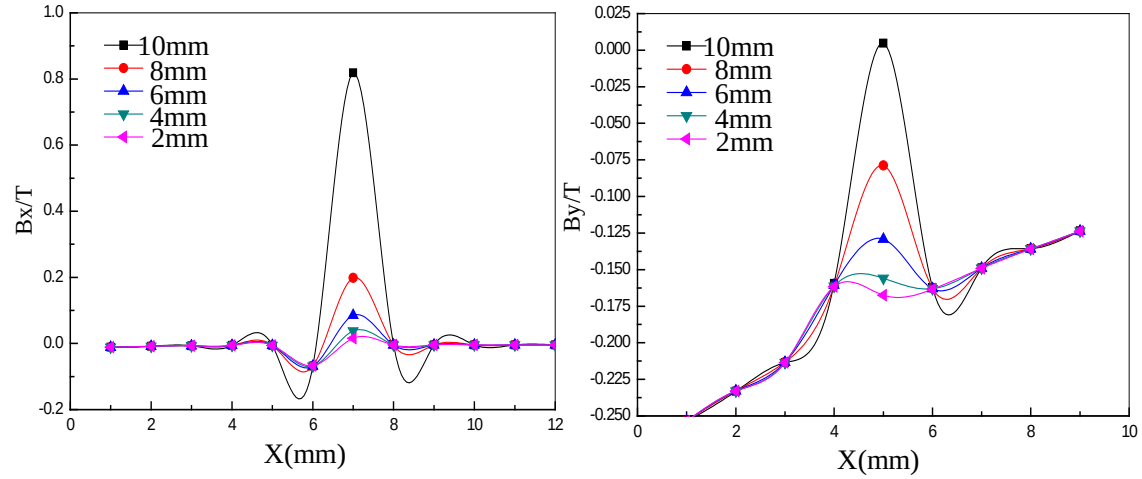

(a)Radial MFL signals of inner defect

(b)Axial MFL signals of inner defect

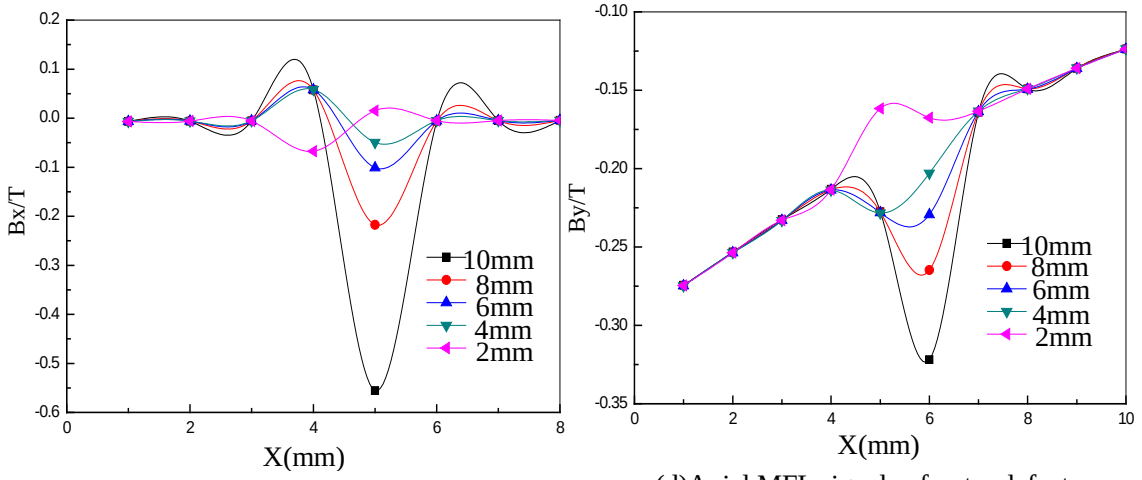

(c)Radial MFL signals of outer defect

(d)Axial MFL signals of outer defect

Fig.5 Weak magnetic field signals dependence on defect width

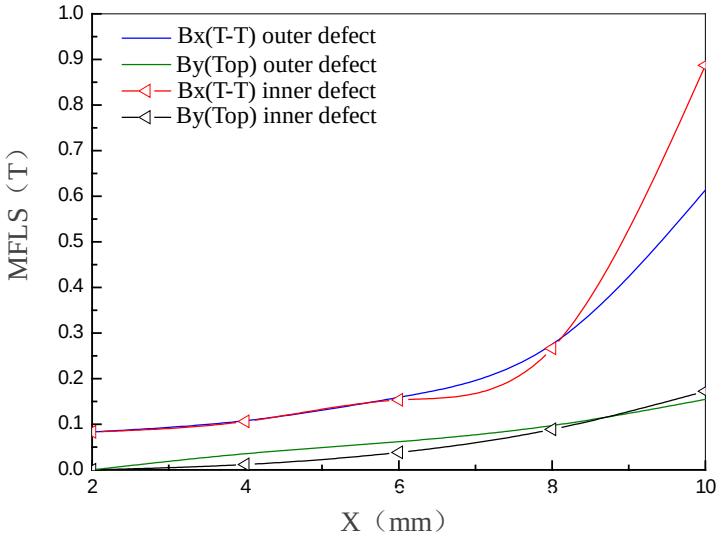

Fig.6 The contrast dependence of defect width

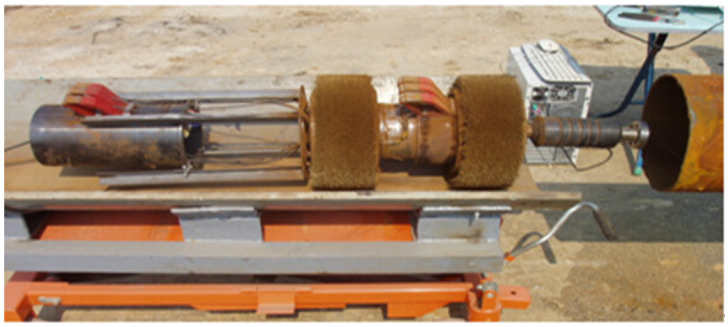

Fig.7 Real MFL Testing Equipment

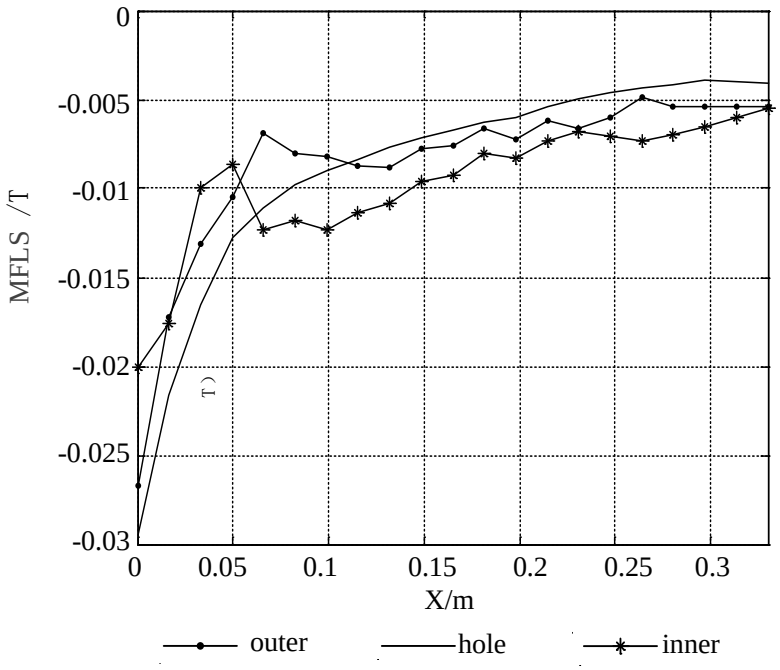

Fig.8Magnetic flux density radial component B_x

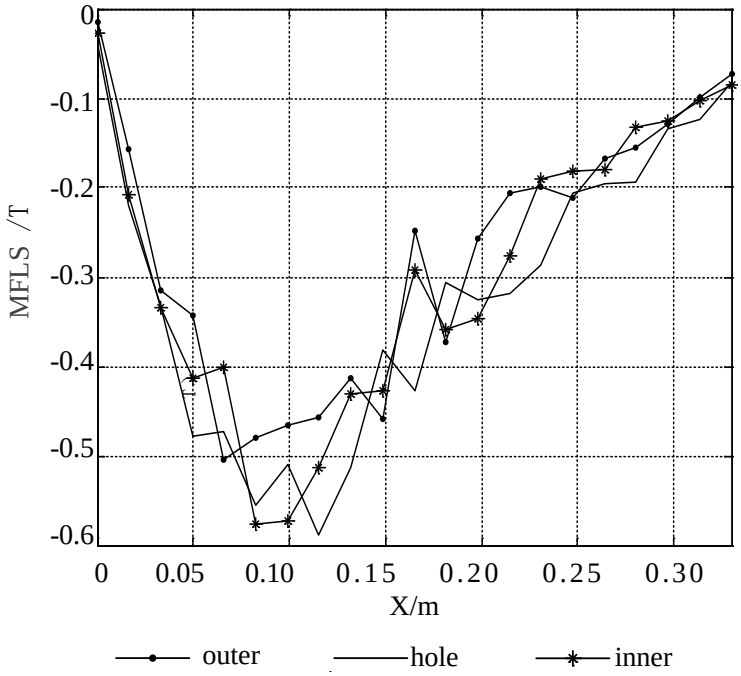

Fig. 9 Magnetic flux density axial component B_y